Obtaining and Characterizing Thin Layers of Magnesium Doped Hydroxyapatite by Dip Coating Procedure

Daniela Predoi, Simona Liliana Iconaru, Mihai Valentin Predoi, Mikael Motelica-Heino, Nicolas Buton, Christelle Megier

coatings

MDPI

Article

Obtaining and Characterizing Thin Layers of Magnesium Doped Hydroxyapatite by Dip Coating Procedure

Daniela Predoi [1,*], Simona Liliana Iconaru [1], Mihai Valentin Predoi [2], Mikael Motelica-Heino [3], Nicolas Buton [4] and Christelle Megier [4]

1 National Institute of Materials Physics, Atomistilor Street, No. 405A, P.O. Box MG 07, 077125 Magurele, Romania; simonaiconaru@gmail.com
2 BN 002, 313 Splaiul Independentei, Sector 6, University Politehnica of Bucharest, 060042 Bucharest, Romania; predoi@gmail.com
3 ISTO, UMR 7327 CNRS Université d'Orléans, 1A rue de la Férollerie, 45071 Orléans, France; mikael.motelica@univ-orleans.fr
4 HORIBA Jobin Yvon S.A.S., 6-18, Rue du Canal, 91165 Longjumeau, France; nicolas.buton@horiba.com (N.B.); christelle.megier@horiba.com (C.M.)
* Correspondence: dpredoi@gmail.com

Received: 15 April 2020; Accepted: 23 May 2020; Published: 27 May 2020

Abstract: A simple dip coating procedure was used to prepare the magnesium doped hydroxyapatite coatings. An adapted co-precipitation method was used in order to obtain a $Ca_{25-x}Mg_x(PO_4)_6(OH)_2$, 25MgHAp ($x_{Mg} = 0.25$) suspension for preparing the coatings. The stabilities of 25MgHAp suspensions were evaluated using ultrasound measurements, zeta potential (ZP), and dynamic light scattering (DLS). Using transmission electron microscopy (TEM) and scanning electron microscopy (SEM) information at nanometric resolution regarding the shape and distribution of the 25MgHAp particles in suspension was obtained. The surfaces of obtained layers were evaluated using SEM and atomic force microscopy (AFM) analysis. The antimicrobial evaluation of 25MgHAp suspensions and coatings on various bacterial strains and fungus were realized. The present study presents important results regarding the physico-chemical and antimicrobial studies of the magnesium doped hydroxyapatite suspensions, as well as the coatings. The studies have shown that magnesium doped hydroxyapatite suspensions prepared with $x_{Mg} = 0.25$ presented a good stability and relevant antimicrobial properties. The coatings made using 25MgHAp suspension were homogeneous and showed remarkable antimicrobial properties. Also, it was observed that the layer realized has antimicrobial properties very close to those of the suspension. Both samples of the 25MgHAp suspensions and coatings have very good biocompatible properties.

Keywords: magnesium; hydroxyapatite; ultrasound measurement; dip coating procedure; antimicrobial activity; cell viability

1. Introduction

During recent years, constant efforts have been made in developing bioceramic materials and enhancing their mechanical and biological properties for use in biomedical applications [1–5]. Due to their properties, bioceramic materials are usually used for developing bone substitutes both in medical and dental applications. The primary uses of calcium phosphate ceramics and calcium phosphate-based composites in dental and medical applications consists in the repair of periodontal defects and dental bone repair as well as in the augmentation of alveolar ridge, dental implants, ear implants, tissue engineering for dental bone grafts, spine fusion and adjuvant to uncoated implants [3–6]. The need for

developing materials that could serve as bone substitutes is strongly argued by the global context in which various bone defects or degenerative bone conditions as well as tumoral resections requiring reconstruction procedures are increasing, and by the facts that more than 500,000 and 1 million bone graft procedures are performed every year in the USA alone and worldwide, respectively [7,8]. Even though noticeable progresses were made in the materials science field, currently, there has not yet been developed a bone substitute that has all the characteristics and properties of an autologous bone and that can be used in vivo with no inflammatory response [6,9,10]. Therefore, at a global scale, there is an ongoing effort in the research area of developing new materials with properties capable of being used in various orthopedic and dental clinical applications. The ongoing studies are focused on developing bone substitutes by tailoring materials having the physico-chemical and structural properties of the natural bone [11]. The development of these types of materials with improved biocompatible and osteoconductive properties will help the process of the bone tissue natural healing [12]. One of the most studied materials for being used as bone grafts are the synthetic calcium phosphate materials. The first successful medical use of calcium phosphates was reported by Albee in 1920 [13], and the first uses of these types of ceramics in dental applications was reported in 1975 by Nery et al. [14]. From the different forms of calcium phosphates, hydroxyapatite, having the general formula ($Ca_{10}(PO_4)_6(OH)_2$), has been the most investigated phase and was extensively researched due to its outstanding biological properties and to its biological response to the physiological environment [15]. Even though hydroxyapatite (HAp) has been extensively used in medical and dental applications because of its resemblance in the chemical composition to the bone mineral matrix [6,12], there are still important differences between the properties exhibited by the natural apatite crystals from the bone mineral and the synthetic conventional hydroxyapatite developed in the laboratory [6,12]. Therefore, research has been conducted in order to enhance the properties of the HAp such as osteoconductivity, osteointegration, mechanical properties, implant efficiency and antimicrobial properties [16,17]. Over the years, several ions such as F^-, Cl^-, Na^+, K^+, Mg^{2+}, Sr^{2+}, Ba^{2+}, Al^{3+}, Mn^{2+}, Cu^{2+}, Zn^{2+}, Ag^+, Ce^{3+}, Eu^{3+}, and Sm^{3+} were used as anion and cation substituents to improve the properties of HAp [18–26]. Among the various metal ions that could be used as dopants in the HAp structure, the most studied ones were Ag+, Sr^{2+}, Zn^{2+}, Mg^{2+}, and Cu^{2+} for their capacity of conferring HAp-elevated biological properties such as osteoconductivity, angiogenity, osteogenicity, and antimicrobial properties as well as improved mechanical properties. However, there are some ions that are known for their role in the biological properties, mostly antimicrobial properties, and for their importance in the biological interactions between a "foreign body "such as an implant and the surrounding tissue. In particular, magnesium is considered to be an excellent choice of an ionic substitutions due to the fact that it has been reported to be the fourth most abundant element in the human body, with a ration between 0.44 and 1.23 wt% and having been found in the bones in a proportion of 0.72 wt% [25,26]. Moreover, magnesium is an essential element found in every living thing and that is necessary for the functionality of all living organisms. More than 100 enzymes are conditioned by the presence of magnesium ions for the catalytic reactions. Furthermore, the absence of magnesium generally induces skeletal affections, a decrease in the osteoblast and osteoclast activities, and is responsible for the apparition of diseases like osteopenia and bone fragility [3,27–30]. Nowadays, there is a great need on the market for the materials that are effective in the replacement or restoration of traumatized damaged or defective bone. The development of such materials is a major clinical and socioeconomic need. In previous decades, various natural and synthetic materials have been proposed for orthopedic application. One of the most studied materials for its exceptional properties was synthetic hydroxyapatite (HAp) [31]. HAp has been explored as substitute in bone grafts due to its close chemical similarity with the inorganic phase of the human bone. Even though it has been extensively used in biomedical applications for artificial bone reconstruction or replacement, most of the time, such constructions of HAp alone failed to serve as efficiently as the natural bone due to its low mechanical strength (brittleness) and inappropriate degradation rate [32]. Therefore, elements with significant biological properties have been chosen as dopants in order to obtain an improved

material based on hydroxyapatite with better mechanical, structural, and biological properties. In this context, ions such as Si, Ag, Mg, Zn, Co, Sr, etc. were investigated to develop new biocomposites based on doped hydroxyapatite. Among them, magnesium is one the most abundant minor element found in biological apatites, and one of the key roles of Mg in the development of bone tissue is related to the adhesion and growth of the osteoblastic cells. Therefore, some studies have reported that doping HAp with magnesium ions will influence the mineral metabolism and will have a great influence also in the dissolution rate of crystals and the biodegradation of the materials [31]. It was also reported [33] that the presence of magnesium from the magnesium doped hydroxyapatite significantly reduces the particle size of the powder compared to normal HAp and greatly improved its mechanical strength [33]. According to the studies conducted by Boanini et al. [34], the results have emphasized that a superior osteoblast proliferation, differentiation, and spreading of the octacalcium phosphate (OCP) doped with 0.6 wt% Mg compared to the control, and even a small concentration of 0.6 wt% Mg, is sufficient to influence the osteoblast behavior.

Therefore, the use of magnesium ions as dopants for hydroxyapatite would constitute the development of a new material with significantly increased biological (osteogenic, osteoconductive, and antimicrobial) and mechanical properties, having explicit influences on the mineral metabolism, on the dissolution rate of the crystals, and also on the biodegradation process [28,29]. Additionally, due to the fact that magnesium has been reported to exhibit antimicrobial properties as well as enhanced osteogenic and angiogenetic properties, the use of magnesium doped hydroxyapatite has been also expanded to the obtaining of biological coatings for dental and orthopedic implants [16,30].

In our previous studies, we reported the stabilities of suspensions based on magnesium doped hydroxyapatite (MgHAp, x_{Mg} = 0.1), magnesium doped hydroxyapatite in the presence of thyme essential oil, and MgHAp nanoparticle suspensions in conjunction with a dextran and thyme solution [30]. We found that the results achieved in the case of the MgHAp nanoparticle suspensions in conjunction with a dextran and thyme suspensions showed that the suspension presented better antimicrobial properties than the anterior reported studies on 10MgHAp (x_{Mg} = 0.1) solutions tested on the same microbial strains at the same time intervals [24]. The increase of antimicrobial activity for MgHAp-based samples in conjunction with a dextran and thyme solution was attributed to both the essential oil and the solution stability increase [30].

In the present study, we aimed to highlight the stability of solutions of magnesium doped hydroxyapatite, $Ca_{25-x}Mg_x(PO_4)_6(OH)_2$, 25MgHAp, when x_{Mg} = 0.25, and to show the homogeneity of the obtained coatings. An evaluation of the antimicrobial properties of the solutions and coatings made was also carried out for the obtained samples when x_{Mg} = 0.25.

2. Materials and Methods

2.1. Materials

$Ca_{25-x}Mg_x(PO_4)_6(OH)_2$ was synthesized using $Ca(NO_3)_2{\cdot}4H_2O$ (calcium nitrate tetrahydrate-Sigma Aldrich, St. Louis, MO, USA, ≥ 99.0%), $(NH_4)_2HPO_4$ (ammonium hydrogen phosphate from Sigma Aldrich, St. Louis, MO, USA, ≥ 99.0%), $Mg(NO_3)_2{\cdot}6H_2O$ (magnesium nitrate hexahydrate, Alpha Aesare, Germany, 99.97% purity), and NH_4OH (ammonium hydroxide, Sigma Aldrich, St. Louis, MO, USA, 25% NH_3 in H_2O). Ethanol absolute and double-distilled water were also used for the synthesis.

2.2. Magnesium Doped Hydroxyapatite (25MgHAp) Suspensions

In order to obtain $Ca_{25-x}Mg_x(PO_4)_6(OH)_2$, an adapted co-precipitation method [35] was used. The synthesis of $Ca_{25-x}Mg_x(PO_4)_6(OH)_2$ was performed at room temperature. The magnesium amount was x_{Mg} = 0.25. In agreement with the previously reported studies [19,36], the molar ratios of Ca/P and (Ca + Zn)/P were equal to 1.67. In order to have the most accurate information regarding the influence of the magnesium quantity both on the stability of the suspension and on the homogeneity of the layers obtained from the suspension obtained, the synthesis conditions presented in one of our

previous studies were respected [24]. The final suspension obtained was called 25MgHA and stirred for 24 h at 100 °C before making the coatings. The 25MgHAp suspension was analyzed using different techniques after stirring at 100 °C for 24 h.

2.3. Thin Layer of 25MgHAp

The 25MgHAp coatings were prepared by dip coating process according to the procedure described previously [37]. Deionized water was used to wash the glass substrate before coating. Three layers of 25MgHAp were deposited on the glass substrate in order to evaluate the homogeneity and uniformity of the deposition as well as the uniform distribution of the constituent elements. Each layer was dried at 80 °C for 4 h. Finally, a thermal treatment was performed at 500 °C for 1 h. Cooling was done at a rate of 5 °C/min.

2.4. Characterization Methods

Ultrasound measurements were performed in agreement with previous studies [38]. For the relevance of the stability of the analyzed suspension, a comparison was made with the properties of double-distilled water. As double-distilled water is the most stable suspension, it was considered a standard suspension, under the same experimental conditions.

Dynamic light scattering (DLS) and zeta potential (ZP) measurements were realized using a SZ-100 Nanoparticle Analyzer from Horiba-Jobin Yvon (Horiba, Ltd., Kyoto, Japan). The measurements were made at 25 ± 1 °C. The distilled water was used to dilute the suspensions before analysis. Ultrasound measurements were performed on concentrated solutions obtained from the preparation process.

Using a CM 20 (Philips- FEI, Hillsboro, OR, USA) transmission electron microscope equipped with a Lab6 filament operating at 200 kV, the samples were investigated using transmission electron microscopy measurements.

A Multimethod SPECS surface analysis system was used to perform X-ray photoelectron spectroscopy measurements (XPS) with monochromatic Al Ka radiation (hv = 1486.6 eV). In the analysis chamber, the vacuum was $p \sim 3 \times 10^{-9}$ torr. For the achievement of XPS spectra, an energy window w = 20 eV with resolution R = 20 eV and 400 recording channels was used. For 25MgHAp coatings, the monochromatic X-ray source (Specs XR-50 M, SPECS Surface Nano Analysis GmbH, Berlin, Germany) was used in the FOCUS mode in order to acquire an X-radiation with a FWHM (Full Width at Half maximum) less than 0.25 eV. The achieved XPS spectra were analyzed and processed using Spectral Data Processor v2.3 (SDP) [39].

The concentration of Mg^{2+} ions released from the 25MgHAp coatings at different time intervals was measured using a laser ablation-inductively coupled plasma-mass spectrometer with an elemental XR Thermo Specific instrument (Waltham, MA, USA). For this purpose, the 25MgHAp coatings were incubated in deionized H_2O and the content of magnesium ions was assessed after 1, 4, 7, and 14 days.

The 25MgHAp suspension morphology and derived coatings were examined using scanning electron microscopy (SEM) with the help of Hitachi S4500 equipment (Hitachi, Tokyo, Japan). The elemental distribution maps and quantitative composition were evaluated with an EDAX (Ametek EDAX Inc Mahwah, NJ, USA) using energy-dispersive X-ray spectroscopy (EDS). Moreover, using ImageJ software (ImageJ 1.51j8, National Institutes of Health, Bethesda, MD, USA), the 3D surface graphics of SEM images could be obtained [40].

The surface morphology of the thin films was characterized by atomic force microscopy (AFM) using a NT-MDT NTEGRA Probe Nano Laboratory instrument (NT-MDT, Moscow, Russia). The topography of the thin film surface was obtained in non-contact mode using a silicon NT-MDT NSG01 cantilever coated with a 35 nm gold layer. Furthermore, the AFM topography was captured on a surface area of 2.5 × 2.5 μm^2, and the root mean square roughness (R_{RMS}) was also calculated. The measurements were performed at room temperature.

Furthermore, the surfaces of the 25MgHAp coatings were also investigated by optical microscopy using a binocular optical microscope with an attached camera from Micros Austria (Micros Austria, Wien,

Austria). The images were recorded using the 40× magnification of the microscope. Complementary information regarding the surface morphology of the 25MgHAp coatings were acquired using an inversed trinocular metallographic microscope OX.2153-PLM, (Euromex, Arnhem, The Netherlands).

The adhesion of the 25MgHAp coatings to the glass substrate was also investigated by tape-pull test using a 3M Performance Flatback Tape 2525 tape with a peel adhesion of 7.5 N/cm.

The qualitative assays of the antimicrobial activity of HAp and 25MgHAp suspensions were carried out as previously described by Predoi et al. [12]. 0.5 McFarland standardized suspensions were inoculated on Muller Hinton agar (MHA). Afterwards, a volume of 5 µL of HAp and 25MgHAp was placed directly, aseptically, and distinctively on the inoculated MHA plates. The plates were then incubated at 37 °C for 48 h and the inhibition zones formed were measured in mm.

The antimicrobial activities of the 25MgHAp suspensions and thin films were assessed against one of the most common and studied microbial strains such as Gram-positive reference strains *Staphylococcus aureus* ATCC 25923, Gram-negative reference strains *Escherichia coli* ATCC 25922, and the reference fungal strain *Candida albicans* ATCC 90029. For this purpose, standard inoculums of each microbial strains of 5×10^6 CFU/mL (colony forming units per milliliter) were prepared. Both 25MgHAp suspensions and 25MgHAp thin films were exposed to 1.5 mL of 5×10^6 CFU/mL microbial suspension in phosphate-buffered saline (PBS) in a Petri dish. Afterwards, the suspension was collected at different time intervals (8, 16, 24, and 48 h) and incubated on agar medium for 24 h at 37 °C. Finally, the number of CFU/mL was determined for each of the contacts. The experiments were performed in triplicate and the results were presented as mean ± standard deviation (SD).

Cell proliferation and viability were evaluated using the MTT (3-4,5-Dimethylthiazol 2,5-diphenyltetrazolium bromide) assay in agreement with previous studies [41]. The in vitro cytotoxicity assessment was carried out using human fetal osteoblasts (hFOB 1.19) from the American Type Culture Collection (ATCC). The absorbance was quantified by measuring the wavelength at 595 nm using a TECAN spectrophotometer (Tecan GENios, Grödic, Germany). The absorbance from the wells of cells cultured in the absence of substrate, coatings, and dispersions was used as the 100% viability value.

2.5. Statistical Analysis

All in vitro experiments were performed in triplicate. The results of the in vitro experiments were exhibited as mean values ± standard deviation (SD). Furthermore, other results of the data were presented as mean values ± standard deviation (SD). For the data analysis, the Student *t*-test was used.

3. Results and Discussion

In the current context, when looking for solutions to improve the quality of life, one of our concerns is the study of the stability of suspensions based on hydroxyapatite doped with different ions that could be used in different applications both in the medical field and in medical food such as would be the development of biocompatible coatings. A complex analysis of the 25MgHAp suspension stability was performed using various techniques such as ultrasound measurements (UM) and zeta potential (ζ potential). Despite the fact that ζ potential is a dedicated method for studying the stability of solutions, the information is obtained by dilution of the concentrated suspensions. For this reason, we have tried to develop a new method for characterizing the stability of the obtained suspensions in concentrated form without having to dilute them.

For a better accuracy of the information regarding the stability of the suspension used in the making of coatings, ultrasonic measurements were made on the concentrated suspension obtained after the preparation process. The digital signals were recorded on the digital oscilloscope at a very precise interval of 5.00 s (Figure 1). As can be seen, we can obtain information both regarding the stability of the suspension and regarding the attenuation vs. time by analyzing the evolution of the signals over time.

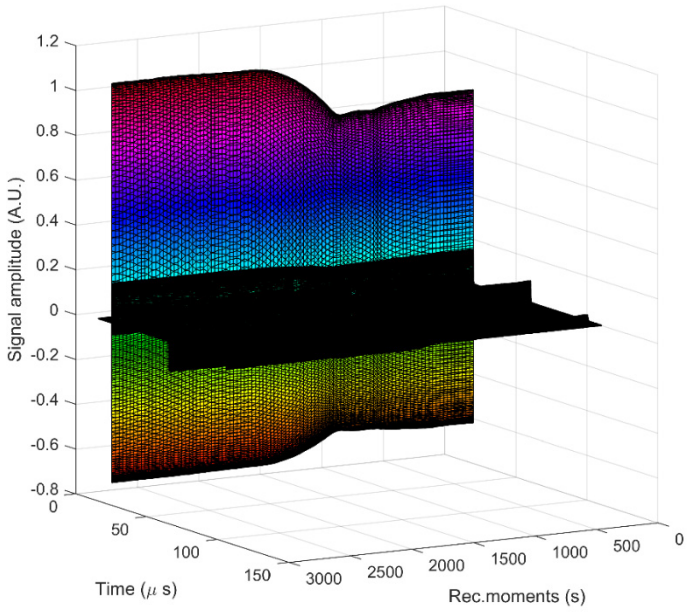

Figure 1. Recorded signals at 5 s recording interval. The increasing amplitudes of the first echo is visible in colors, whereas the second and third echo are significantly weaker (in black).

Time delays between the first three echoes that were recorded in the analyzed suspension and those recorded in the reference fluid allowed a precise determination of the velocity of ultrasounds through the sample for each signal that was recorded. The result for the velocity in the reference fluid was c_0 = 1496.19 m/s, while the velocity in the analyzed sample was c = 1496.84 m/s and the temperature at which the experiment was performed was 24.8 °C. The ultrasound velocity in the sample is very close to the velocity in pure water and has a negligible variation during the experiment. Thus, it cannot be used to characterize the evolution in time of the sample's properties.

A more significant variation is determined by the maximum amplitudes of transmitted signals vs. recording moments (Figure 2). There is a very slow variation of the amplitudes for $t < 500$ s which will be used for further processing, followed by a more pronounced variation of the amplitudes up to 1000 s. Between recording moments 1000 and 1700 s, as the apparent surface of sedimentation passes in front of the coaxial transducers, a rapid variation of amplitudes occurs. An unusual increase of the second echo amplitude above the amplitude of the first echo is specific to this sample. After this passage, it follows a long sedimentation period ($t > 1600$ s), in which the echoes amplitudes tend asymptotically to those in the reference fluid ($A/A_{\text{ref}} \rightarrow 1$).

In order to evaluate the stability of the suspension, the first period ($t < 100$ s) has the greatest relevance. The amplitude of the first echo was measured with very good accuracy. It was observed that, during this period, the amplitude of the first echo shows a slow decrease. The parameter that gives us clear information on the stability of the suspension is closely related to the slope of the amplitude of the first echo vs. time.

The value of the stability parameter was $s = \frac{1}{A_m}\left|\frac{dA}{dt}\right| = 0.019\ \text{s}^{-1}$ with A_m the averaged amplitude of the signals. The value obtained for the stability parameter shows a good stability of 25MgHAp suspension. Another characteristic of the suspension is the frequency spectrum of the first transmitted echo (Figure 3). The lowest curves correspond to the first period of sedimentation and the upper ones correspond to the asymptotic sedimentation of the suspension fluid, during which the amplitudes increase. The peaks of amplitudes are at 4 MHz, which is a characteristic of the transducers. Combined information of the previous two figures leads to the spectral amplitudes variation during the experiment. On Figure 4 is shown the initial highest amplitude ratio of 0.95 for the frequency of 2 MHz and the lowest of 0.7 at 8MHz. All values are relative to those of the reference fluid in the same conditions. Before t = 1050 s, the amplitudes at all selected frequencies are slowly decreasing. After the separation

surface descends in front of the transducers, these amplitudes tend to 1, which is normal for a complete sedimentation.

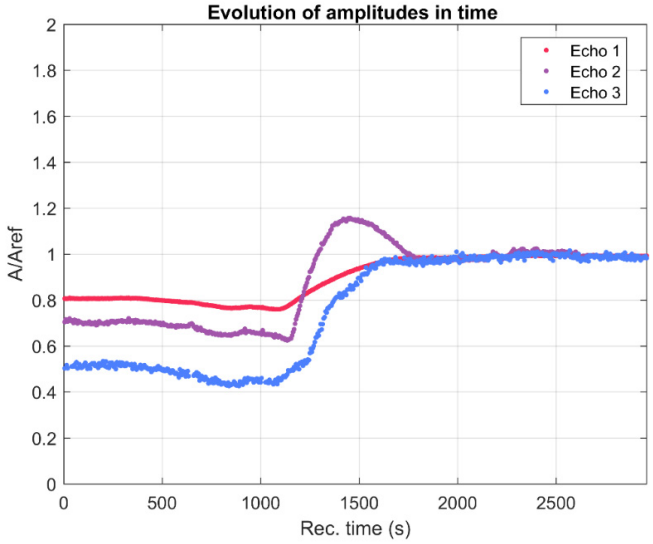

Figure 2. Relative amplitudes evolution vs. the recording moments.

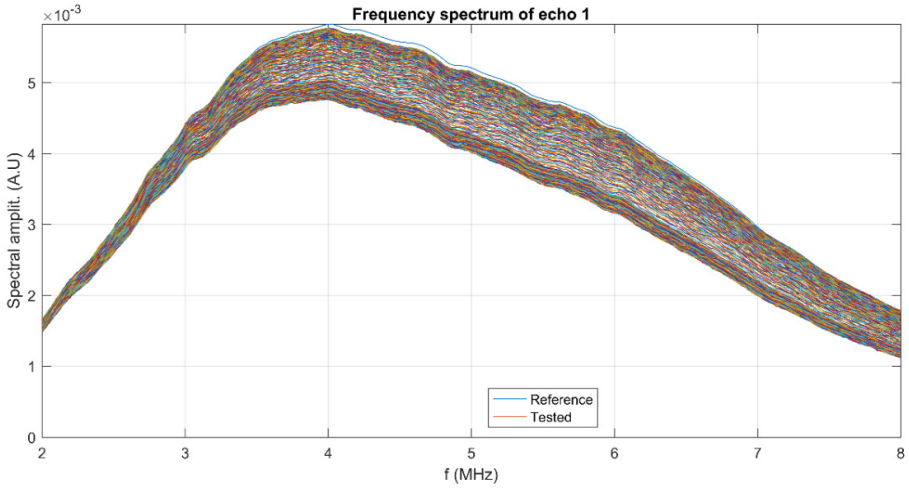

Figure 3. Frequency spectrum of the first transmitted echo.

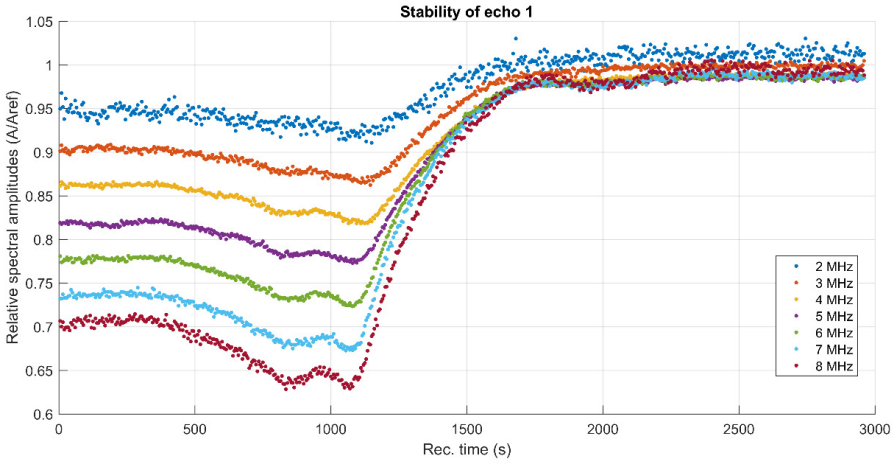

Figure 4. Spectral amplitudes of relative variation vs. time for the first echo.

As proved in Figure 5, the attenuation calculated for each spectral component depends on the moment during the experiment. The attenuation of bidistilled water used as reference fluid for each spectral component was also presented in Figure 5. The bidistilled water used as the reference fluid comportment was represented in dashed lines with the same colors legend. A specific feature of the 25MgHAp suspension is the attenuation equal to 13.5 nepper/m for the 8 MHz component in the first moments of recording a first echo. For the 25MgHAp suspension, the lowest attenuation of 2 nepper/m was obtained for the 2 MHz spectral component.

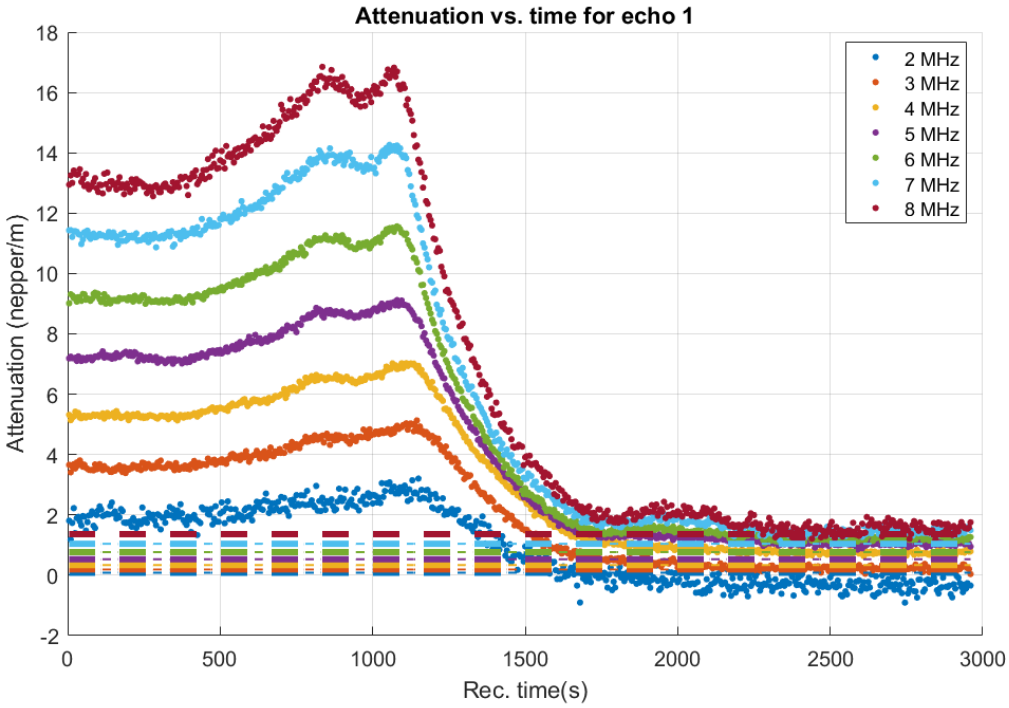

Figure 5. Attenuation vs. frequency for the first transmitted echo. The reference fluid is depicted in dashed lines with the same color legend.

Figure 6 shows the attenuation dependency of frequency for both the 25MgHAp suspension and the reference fluid. As can be seen in the case of the analyzed suspension, the attenuation is considerably higher (1–7 nepper/m) compared with the reference fluid (0.3–1.3 nepper/m).

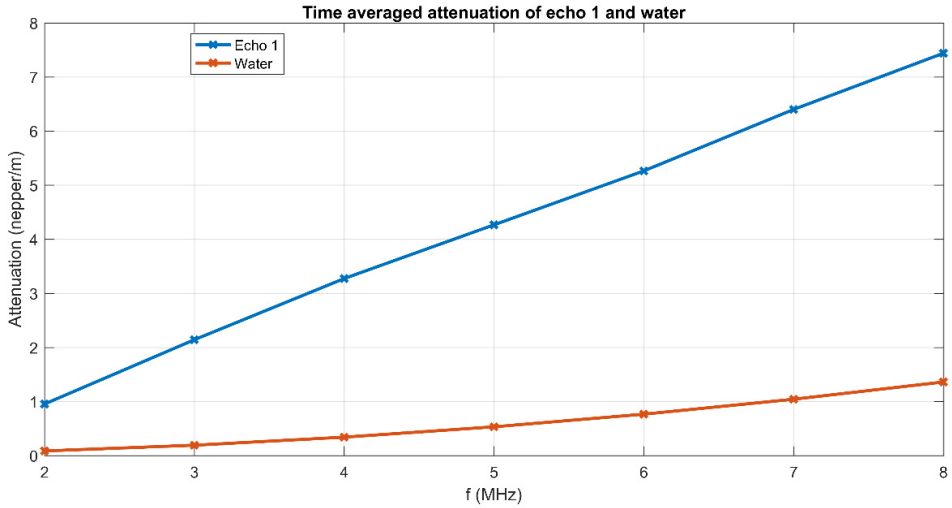

Figure 6. Attenuation vs. time for the spectral components of echo 1.

The attenuation is increasing in time (t < 1050 s) for all spectral components of the signal, expressing an increasing concentration of the suspension. The attenuation decreases progressively, as the suspension is settling and the separation surface passes in front of the transducers.

Following these studies, it was found that, for the 25MgHAp suspension, the attenuation coefficients tend towards stable values during the long period of asymptotic sedimentation (after 1700 s in this case). The stable values at which the attenuation coefficients of the 25MgHAp suspension correspond to the values obtained for bidistilled water used as the reference fluid. The complete process lasted more than 2000 s before a final stable state was reached. The present studies confirm that the first transmitted echo (recorded in the first 500 s) provides sufficient information for a rigorous and complete characterization from the ultrasonic point of view of the 25MgHAp suspension in terms of stability, total, and spectral attenuation.

In order to evaluate the particle distributions and physical stabilities of the nanosuspensions, the DLS and ζ potential studies were conducted (Figure 7). In order to highlight the particle distribution in the suspension used for coating, DLS studies were performed. Figure 7a revealed dynamic light scattering data by volume of 25MgHAp particles obtained from the prepared suspension. The intensity distribution was converted to volume distribution by using scattering theories of Mie. The volume distribution profiles revealed a single peak, which shows that the aggregates of the nanoparticles in the analyzed suspension were negligible. The sizes of 25MgHAp particles coming from suspension vary in the range 10–90 nm, with a mean value of hydrodynamic diameter, D_h, equal to 22 nm. On the other hand, determination of ζ potential is a significant technique for characterizing the suspensions, allowing us to understand the physical stability of the nanosuspensions. In this context, the stabilities of the 25MgHAp suspensions were also analyzed using ζ potential determination. The ζ potential distribution achieved for the 25MgHAp suspension was presented in Figure 7b. The value obtained for the ζ potential following the measurements was −32.9 ± 3.4 mV, indicating a good stability of the 25MgHAp suspension. According to J.P. Kadu et al. [42], when for the ζ potential we have values greater than 30 mV and less than −30 mV, we can talk about good stability. Moreover, Mohapatra et al. [43] showed that a confirmation of the particle agglomeration in the suspension is confirmed when the ζ potential has negative values less than −28 mV and positive values less than 28 mV. On the other hand, E. Joseph and G. Singhvi [44] showed that suspensions with values of ζ potential greater than 30 mV or less than −30 mV have high stability degrees while, when the suspensions for which the ζ potential has a value of less than +25 mV or greater than −25 mV, they will eventually agglomerate due to interparticle interactions, including van der Waals forces and hydrogen bonding. Besides, in our anterior study [24], we certified with ultrasound measurements that a value of −17 ± 3.4 mV of ζ-potential obtained for 10MgHAp in water indicates that the suspension is unstable. Moreover, in recent studies on "Dextran-thyme coated magnesium doped hydroxyapatite layers on glass substrate" [30], ultrasound measurements confirmed that, for a value of −37 mV of the ζ-potential, the suspension has a good stability.

By the results obtained in the present study, we have shown that by increasing the amount of magnesium in the sample x_{Mg} = 0.25, the suspension stability has increased compared to previous results [24] when the amount of magnesium in the sample was x_{Mg} = 0.1. The studies performed using ultrasound measurements (on concentrated samples) have confirmed that the stability of the suspensions improved when the amount of magnesium increased from x_{Mg} = 0.1 to x_{Mg} = 0.25 by decreasing the stability parameter from 0.087 to 0.019 s^{-1}.

The morphology of the 25MgHAp particles in suspension were estimated using TEM and SEM analysis. From the TEM and SEM images realized on the 25MgHAp suspension shown in Figure 8, it was noticed that the particles have a uniform shape. The TEM and SEM examination revealed that the 25MgHAp particles in suspension appear as regular spherical structures at the nanometer scale. The average particle size obtained for the 25MgHAp sample was 12.7 ± 2.5 nm from TEM, while from SEM measurements, it was about 15.3 ± 3.4 nm (Figure 8). The TEM results were in good concordance with those obtained from the SEM studies.

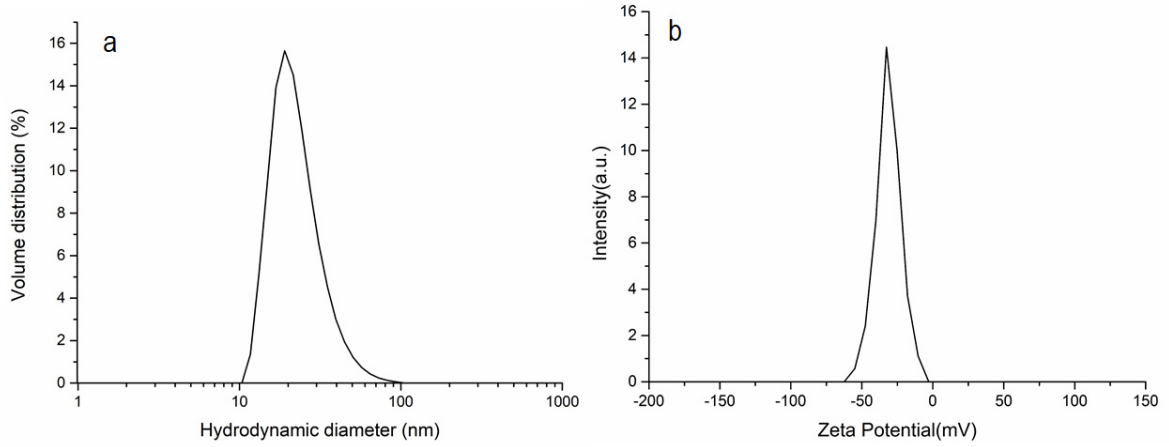

Figure 7. Hydrodynamic diameter, D_h, distribution by volume (**a**) and ζ-potential (**b**) of 25MgHAp nanoparticles in suspension.

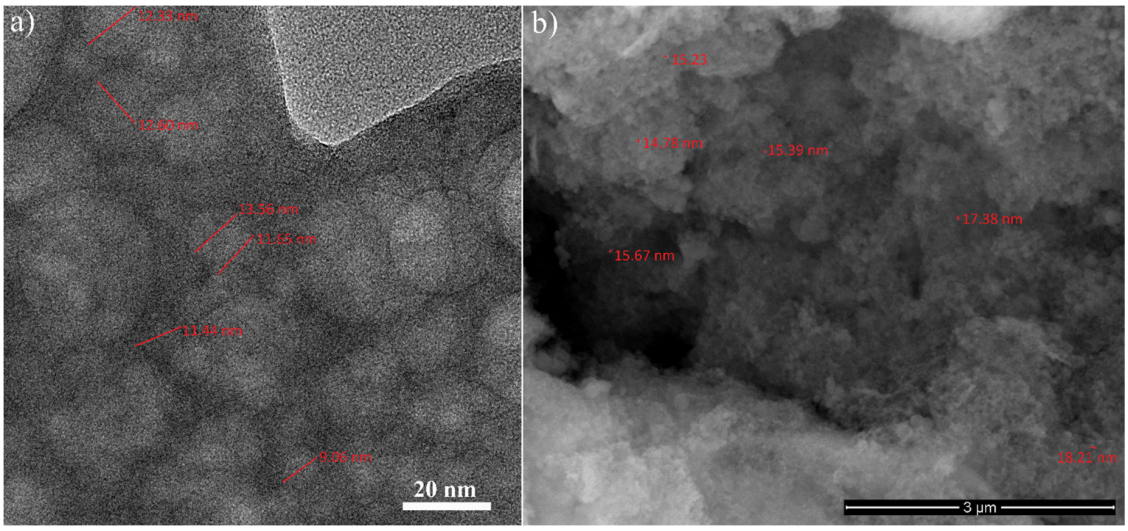

Figure 8. TEM (**a**) and SEM (**b**) images of 25MgHAp particles in suspension.

To confirm the homogeneity of the coating, four complementary methods of analysis were used. The mapping analysis of the 25MgHAp coatings obtained using the dip coating method showed a homogeneous surface (Figure 9a). Figure 9b–e clearly exhibited the presence of Ca, P, Mg, and O elements. On the other hand, from the mapping images, it was observed that all the constituent elements were uniformly distributed on the surface of the 25MgHAp coatings. The superposition of all constituent elements of the surface of the 25MgHAp coatings was also presented in Figure 9f. In order to evaluate the elemental composition of the 25MgHAp coatings, energy dispersive X-ray spectroscopy (EDS) was performed. In the EDS spectra that were identified, only the constituent elements of the magnesium doped hydroxyapatite (O, Ca, P, and Mg) were observed. The presence of Si in the EDS spectrum was due to the substrate. The result of the EDS analysis attests a good purity of the coatings. The EDS spectra of the 25MgHAp coating surface is presented in Figure 9h.

Furthermore, the 2D conventional SEM and EDX mapping images were transformed into 3D surface maps using ImageJ software (ImageJ 1.51j8, National Institutes of Health, Bethesda, MD, USA) [40] and the 3D representations are depicted in Figure 10. The 3D representations of the SEM surface topographies suggested the presence of a uniform layer with no fissures or other imperfections. In addition, the 3D surface maps of the elemental cartographic analysis highlighted that the main constituents of the magnesium doped hydroxyapatite, O, Ca, P, and Mg, were homogenous and uniformly distributed in the analyzed sample.

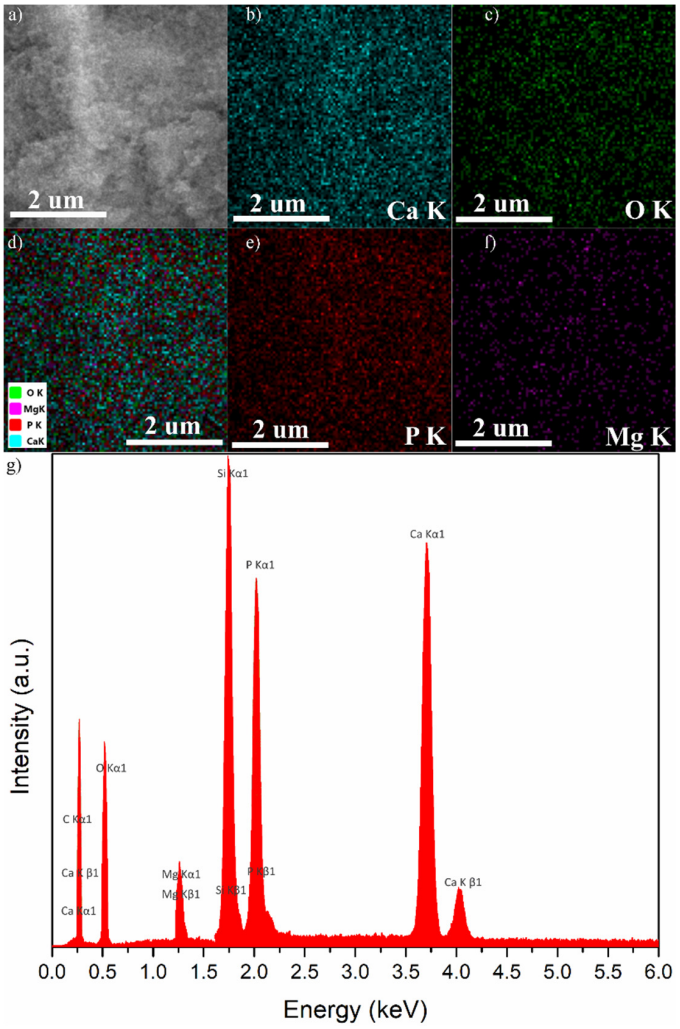

Figure 9. SEM image (**a**), mapping analysis of Ca (**b**), P (**c**), Mg (**d**), O (**e**), superposition of all constituent elements (**f**), and EDS spectra (**g**) of the 25MgHAp coatings surface.

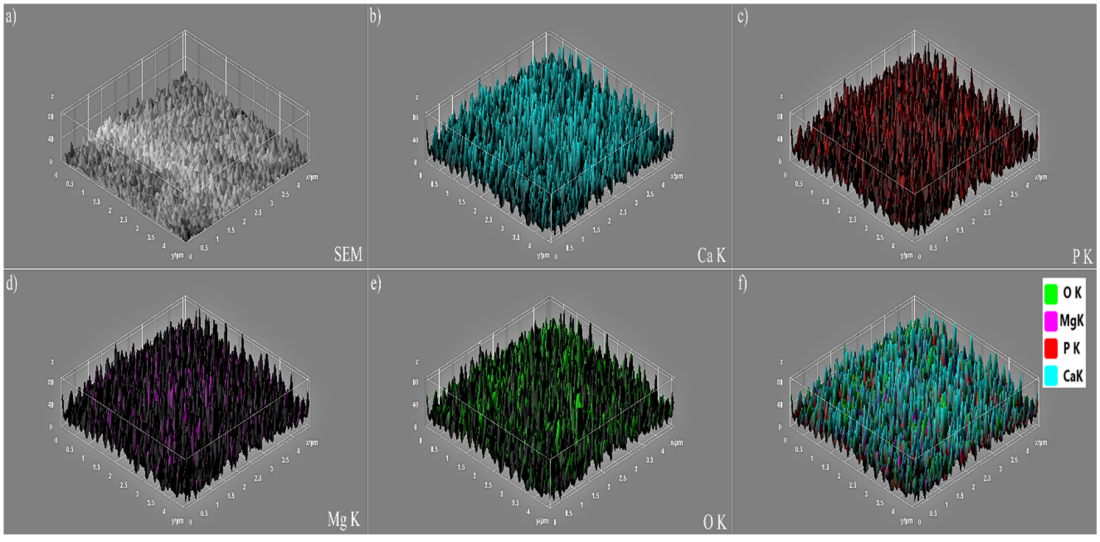

Figure 10. 3D representation of SEM image (**a**), mapping analysis of Ca (**b**), P (**c**), Mg (**d**), O (**e**), and superposition of all constituent elements (**f**) of the 25MgHAp coatings surface.

Complementary information regarding the magnesium ions released from the 25MgHAp coatings were obtained by incubating the 25MgHAp coatings in deionized water and measuring the Mg^{2+} ions concentration of the solution after 1 day, 4 days, 7 days, and 14 days by inductively coupled plasma mass spectrometry. The results of the Inductively Coupled Plasma Spectrometry (ICP) studies revealed that after 1 day in the solution in which the 25MgHAp coating was immersed, the concentration of Mg^{2+} was 5.2 ± 0.8 mg/L. After 4 days, its concentration had a value of 15.4 ± 1 mg/L, and after 7 days, the magnesium ions reached a concentration of 18.24 mg/L. Furthermore, after 14 days, the concentration of Mg^{2+} ions released from the 25MgHAp coatings had a value of 18.84 mg/L. These results suggested that the release of magnesium ions from the 25MgHAp coatings increased progressively in the first 7 days and then in the next 7 days had a slow increase.

Moreover, the thickness of the 25MgHAp layers was assessed using SEM analysis. The SEM analysis of the transversal cross section of the investigated layers indicated a thickness equal to 56.04 ± 2.4 nm. The results are depicted in Figure 11.

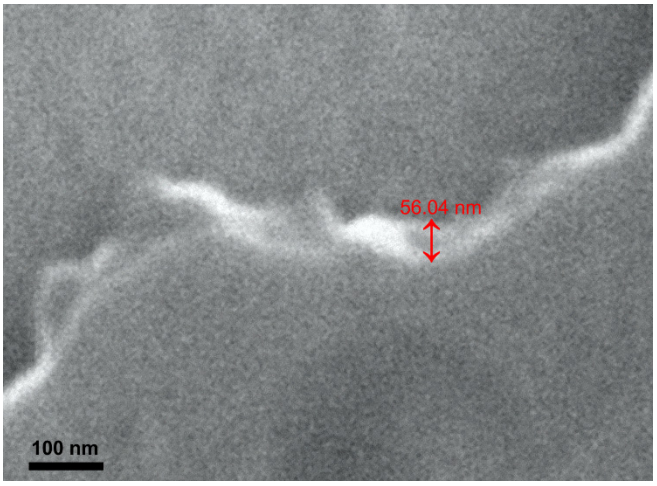

Figure 11. SEM images of the transversal cross section of 25MgHAp coatings.

Furthermore, the adhesion of the 25MgHAp coatings to the glass substrate was investigated using the tape-pull test. The tape-pull test is one of the simplest and most widely used method to evaluate a coating's adhesion. In the case of the 25MgHAp coatings deposited on glass substrate, the scotch tape came off relatively clean with very little material stuck to it, and the analysis of the substrate surface suggested that not much of the 25MgHAp coating was actually removed. These results indicated a good adhesion of the thin layer to the substrate.

The surface morphology of the 25MgHAp thin films was also investigated using AFM analysis. The AFM topography of the 25MgHAp coatings surface is presented in Figure 12. The AFM 2D micrograph and the 3D representation of the 25MgHAp coatings surface emphasized that the 25MgHAp coatings surface has the morphology of a uniformly deposited layer. Moreover, the AFM topography also suggested that the thin film do not present any cracks or fissures and consist of nanoaggregates. In addition, the AFM results evidenced that the surface topography of the 25MgHAp coatings was also homogenous with a roughness (R_{RMS}) value of 47.34 nm. The results obtained by AFM investigations are in agreement with the SEM studies, which also revealed that the coatings are uniform and homogenous.

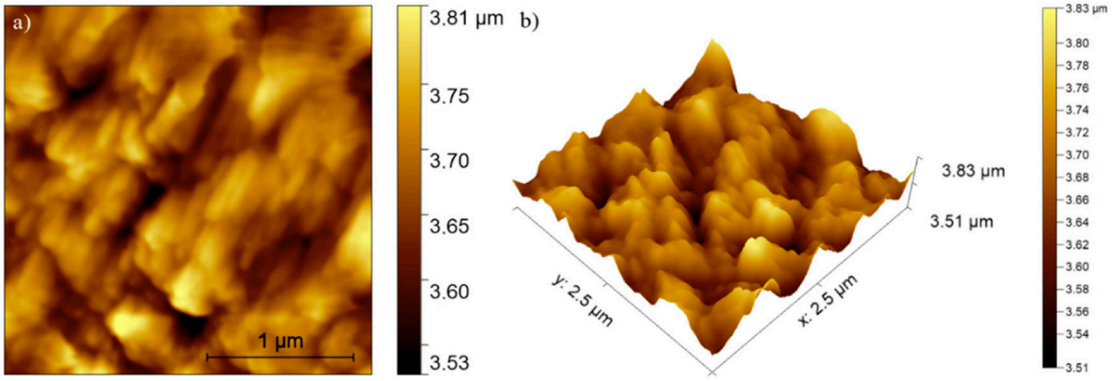

Figure 12. Atomic force microscopy (AFM) topography image of the 25MgHAp thin film surface presented in 2D (**a**) and 3D representation of the surface topography of 25MgHAp thin film (**b**).

Furthermore, the surface morphology of the 25MgHAp coating was studied using optical and metallographic microscopy. The images acquired with the optical microscope of the surface morphology of the 25MgHAp coatings are presented in Figure 13a. The optical images of the surface of the 25MgHAp coatings revealed that the coatings deposited by dip coating process are uniform with no visible fissures, cracks or other visible discontinuities. Moreover, a 3D representation of the optical image of 25MgHAp coating's surface was obtained using ImageJ software (ImageJ 1.51j8, National Institutes of Health, Bethesda, MD, USA) [36]. The 3D representation of the optical image of 25MgHAp coating is depicted in Figure 13b.

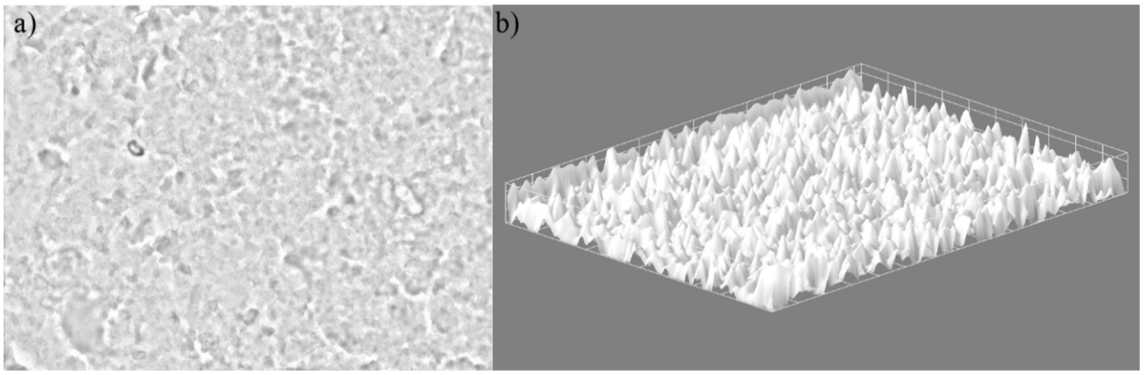

Figure 13. Optical microscopy image of the 25MgHAp surface coatings (**a**) and 3D representation of the surface of the 25MgHAp coatings (**b**).

Complementary information regarding the surface morphology of the 25MgHAp coatings were also obtained using metallographic microscope. The image of the 25MgHAp coating's surface obtained using the metallographic microscope is depicted in Figure 13a. As well as the optical microcopy studies, the metallographic investigations revealed that the surface of 25MgHAp coatings has a uniform morphology and do not present any fissures or cracks. In addition, a 3D representation of the 25MgHAp coating surface was also obtained with ImageJ software (ImageJ 1.51j8, National Institutes of Health, Bethesda, MD, USA) [40]. The 3D representation of the metallographic microscope image of the 25MgHAp coating surface presented in Figure 14b emphasized and confirmed that the 25MgHAp coatings are homogenous and continuous with no cracks or fissures. Following the studies performed using four methods of analysis such as SEM, AFM, optical microscopy, and metallographic microscopy, we can say that the coatings obtained are homogeneous and do not show cracks.

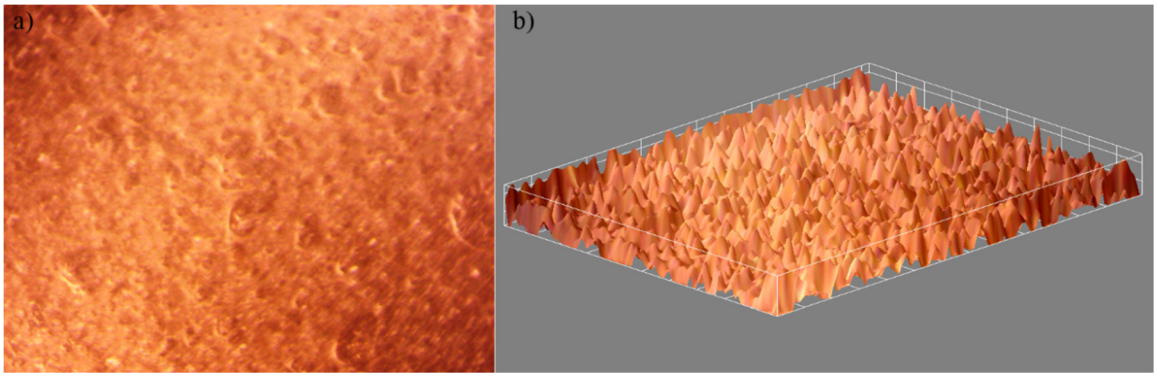

Figure 14. Metallographic microcopy image of the 25MgHAp coating surface (**a**) and 3D representation of the surface of the 25MgHAp coatings (**b**).

Furthermore, the roughness parameters R_a of the coating surfaces were also calculated using AFM, SEM, optical microscopy, and metallographic microscopy images of the surface coatings. R_a is one of the most commonly used parameters in industry to characterize the roughness of a surface. R_a represents the average of a set of individual measurements of the peaks and valleys of a surface. The arithmetic average of the absolute values of the profile height deviations from the mean line of the 25MgHAp coating surface images was determined using optical analysis of the images using ImageJ software [40]. The numerical values of the R_a roughness parameters determined from different 25MgHAp surface images are presented in Table 1. The results highlighted that that the R_a roughness parameter calculated from AFM, SEM, optical microscopy, and metallographic microscopy images of the 25MgHAp surface coatings had similar values and were in accordance with the visual analysis of the coating's surface from the optical and metallographic images.

Table 1. R_a roughness parameters of 25MgHAp coatings.

Image	R_a (nm)
AFM	119 ± 2.4 nm
SEM	121 ± 4.6 nm
Optical microscopy	183 ± 6.8 nm
Metallographic microscopy	133 ± 8.2 nm

Figure 15 showed the high resolution Mg 1s and Mg 2p XPS spectra of 25MgHAp coatings. In Figure 14a, the high resolution Mg 2p XPS spectra of 25MgHAp coatings were presented. The metallic component at the binding energy (BE) around 1303 eV was not observed. The binding energy of Mg 2p is slightly higher than that of the oxide. The peak at 1305 eV could indicate the bonds of Mg^{2+} with the PO_4^{2-} group. The Mg 2p XPS spectra revealed a single peak at around 50.32 eV (Figure 15). A peak associated with metallic magnesium around 49 eV was not observed [45]. In agreement with S. Ardizzone et al. [46], the BE of Mg 2p ranges between 49.9 and 50.2 eV. Thus, the peak at 50.34 eV may indicate the bonds of Mg^{2+} with the PO_4^{2-} group. In the sample studied, the Ca^{2+} was substituted by Mg^{2+}. The low intensity of this region reflects the low level of oxygen contamination of the 25MgHAp coatings [47].

Recently, due to the emergence of various drug resistant microbial strains, the focus of the research communities has been towards developing new antimicrobial agents. Among the resistant microbial strains, the most prominent are Gram-positive and Gram-negative bacterial strains such as *Staphylococcus aureus* and *Escherichia coli* which have developed resistance to a wide range of antibiotics used as conventional antimicrobial treatments. Therefore, in surgery, it is very important to have a sterile environment around the implant. One of the most studied materials for its outstanding

biocompatible properties that was envisaged by the researchers for being used in the development of new antimicrobial agents was HAp doped with different antibiotics or antimicrobial components. These modifications were expected to facilitate its use in bone substitutions and in the case of infected bone defects.

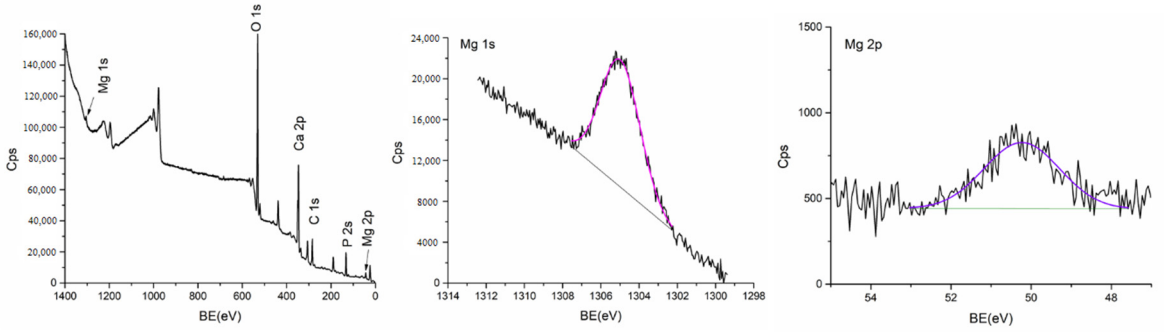

Figure 15. The XPS survey spectrum of the 25MgHAp coatings. High resolution Mg 1s and Mg 2p spectra of 25MgHAp coatings.

The antimicrobial activities of the HAp and 25MgHAp suspensions have been assessed by determining the mean zone of inhibition produced by the samples after 48 h of incubation with the microbial cultures. The results have emphasized that the HAp suspensions did not show any antimicrobial activity after 48 h of incubation in the presence of microbial cells against Gram-positive *Staphylococcus aureus* ATCC 25923, Gram-negative *Escherichia coli* ATCC 25922, and fungal *Candida albicans* ATCC 90029. The results are depicted in Figure 16. Furthermore, the results of the qualitative antimicrobial assay have shown that the 25MgHAp suspensions presented significant antimicrobial properties against the tested microbial strains. The results evidenced that the 25MgHAp suspensions presented different zones of inhibition particular to each microbial strain. After 48 h incubation with 25MgHAp suspensions for the *S. aureus* culture, the mean zone of inhibition was 17.4 ± 0.8 mm, while in the case of *E. coli*, the mean zone of inhibition was 21.7 ± 1.2 mm, and for *C. albicans*, the results revealed a mean zone of inhibition of 28.7 ± 0.6 mm. The results highlighted that the 25MGhAP suspensions were the most efficient towards development of the fungal cell *C. albicans*.

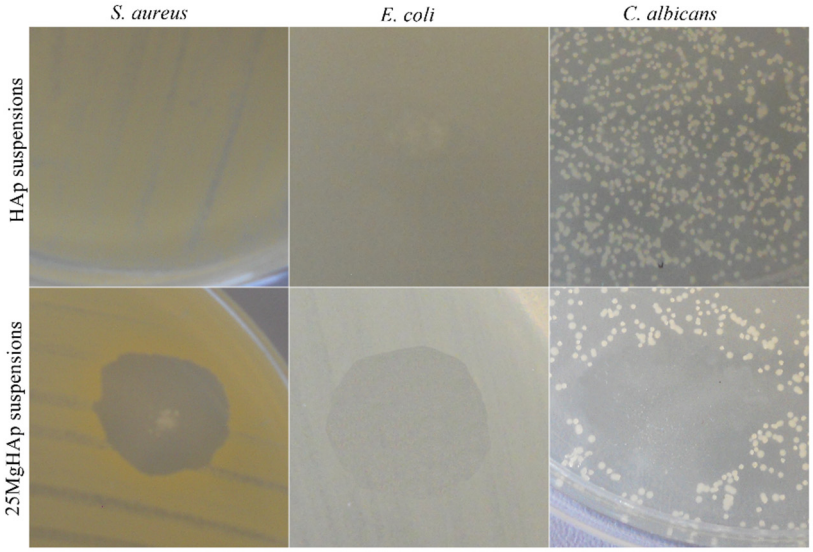

Figure 16. Antimicrobial qualitative assay of HAp and 25MgHAP suspensions against *Staphylococcus aureus* ATCC 25923, *Escherichia coli* ATCC 25922, and *Candida albicans* ATCC 90029.

In the present study, the antimicrobial efficiencies of 25MgHAp and HAp suspensions as well as 25MgHAp and HAp coatings against the development of microbial cells against Gram-positive *Staphylococcus aureus* ATCC 25923, Gram-negative *Escherichia coli* ATCC 25922, and fungal *Candida albicans* ATCC 90029 were investigated. The antimicrobial activities of the samples against the tested microbial strains were tested at various time intervals. The results of the antimicrobial assays regarding the inhibitory effect against the development of CFU in the presence of the 25MgHAp and HAp suspensions as well as 25MgHAp and HAp coatings are depicted in Figure 17a,b. The antimicrobial assays have revealed that the best inhibitory effect was obtained in the case of *Candida albicans* ATCC 90029. Moreover, the effectiveness of both the 25MgHAp suspensions and 25MgHAp coatings against *Staphylococcus aureus* ATCC 25923 and *Escherichia coli* ATCC 25922 was proved. The results of the antimicrobial assay also evidenced that HAp suspensions did not inhibit the growth of the tested microbial cells. Moreover, the results have emphasized that the HAp suspensions have been a good environment for the proliferation of the *Staphylococcus aureus* ATCC 25923, *Escherichia coli* ATCC 25922, and *Candida albicans* ATCC 90029 microbial strains. Additionally, the results suggested that the 25MgHAp suspensions and coatings were more efficient against the tested bacterial strains compared to pure hydroxyapatite samples. Furthermore, the results of the antimicrobial assays demonstrated that the 25MgHAp suspensions exhibited fungicidal properties after 48 h of incubation with the *C. albicans* ATCC 90029 fungal strains. Moreover, the data suggested that the samples started inhibiting the CFU development for all tested strains from 8 h of incubation. These results are in good agreement with our previous studies regarding the influence of magnesium doped hydroxyapatite suspensions and magnesium doped hydroxyapatite enhanced with thyme essential oil in dextran matrix solutions and composite layers on the development of microbial biofilms [24,30]. The results obtained in our previous reported studies [30] suggested that the 10MgHAp-Dex-thyme suspensions presented strong antimicrobial properties even after 24 h in the case of Gram-negative *P. aeruginosa* and Gram-positive *S. aureus* bacterial strains. In addition, the results presented in the study regarding "dextran-thyme magnesium-doped hydroxyapatite composite antimicrobial coatings" [30] emphasized that 10MgHAp-Dex-thyme layers exhibited a good antimicrobial effect against the formation of the microbial biofilm after 24 h of incubation against Gram-negative *P. aeruginosa* and Gram-positive *S. aureus*. Nonetheless, the results reported in the previous studies of the authors on the antimicrobial activity of the dextran-thyme magnesium-doped hydroxyapatite composite coatings [30] demonstrated that the antimicrobial properties were more pronounced in the case of 10MgHAp-Dex-thyme suspensions than in the case of 10MgHAp-Dex-thyme layers for all tested time intervals compared to the control sample. In this context, the results obtained in the case of the 25MgHAp suspensions and 25MgHAp coatings efficiency in inhibiting the development of CFU of different microbial strains are in perfect agreement with our previous studies, and demonstrated that the 25MgHAp suspensions proved more efficient against the development of CFU of the tested microbial cells compared to the 25MgHAp coatings. Furthermore, in our previous studies [24,30], we have demonstrated that HAp suspensions presented a stimulating effect on the microbial biofilm development, therefore, the antimicrobial effect exhibited by the magnesium doped hydroxyapatite suspensions and thin films could be attributed entirely to the magnesium presence. These results were also confirmed in our present study, which highlighted that, after 16 h of incubation, the HAp suspensions had facilitated the proliferation of the microbial cells. A noticeable increase in the CFU values of the microbial strains incubated with the HAp suspensions was observed after 16 h of incubation. In addition, the results also suggested that the HAp coatings exhibited a very small inhibiting effect after 24 h of incubation in the case of *S. aureus* and *C. albicans* microbial cells. This limited antimicrobial effect could be attributed to the presence of silicium ions from the glass substrate and also to the interactions that appeared between the HAp coatings and glass substrate [48]. Although some antimicrobial properties of simple glass were reported, there are only few existing studies regarding this aspect and there is much to investigate in order to fully understand the mechanism involved. [48,49]. These findings are also in good agreement with the literature [30–35,49–54]. The principal mechanisms

involved in the antimicrobial activity of magnesium-based materials have been described as similar to the ones encountered in the case of other metallic ions. Therefore, the literature revealed that, generally, nanoparticles are toxic to organisms by generating oxidative stress, inflammation, or by inflicting direct or indirect DNA damage [51,52], and also by producing reactive oxygen species (ROS), which are responsible for inducing oxidative DNA damage, protein denaturation, and lipid peroxidation [51,52].

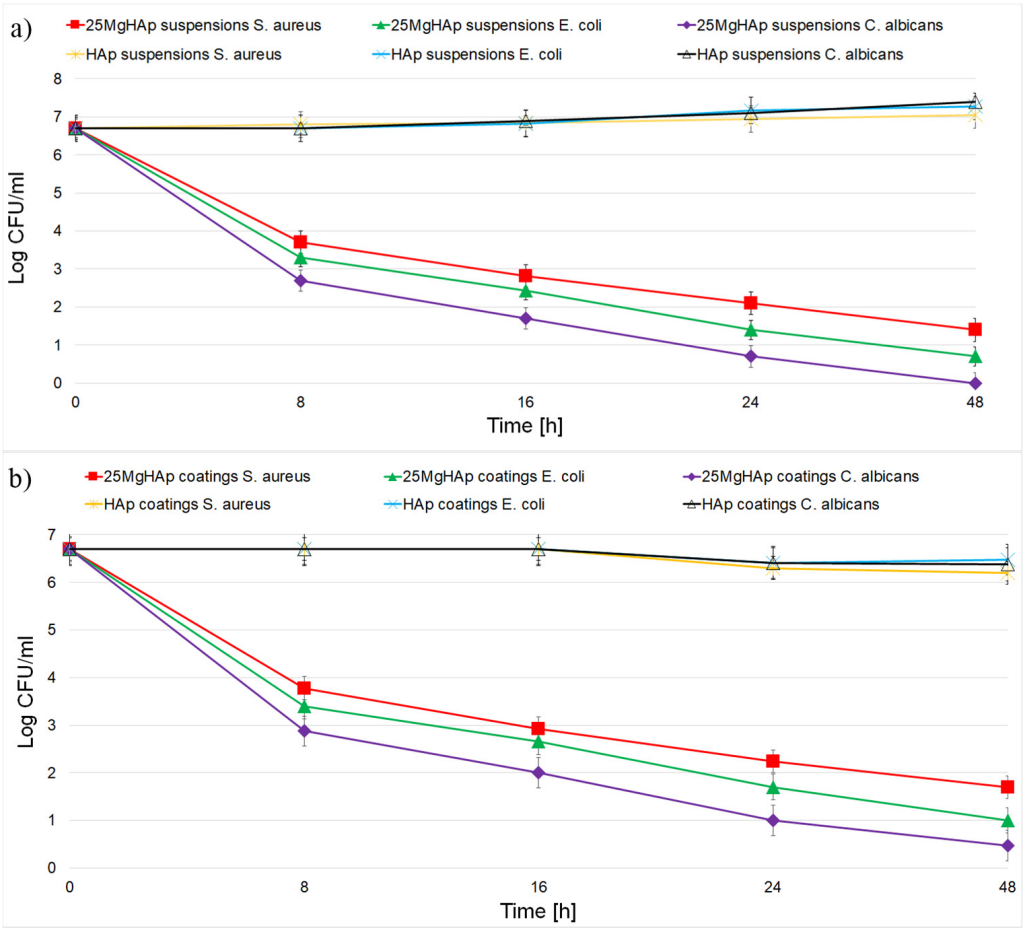

Figure 17. The graphical representation of the Log CFU/mL as a function of time of exposure to the 25MgHAp suspensions (**a**) and 25MgHAp thin films (**b**).

In addition to antimicrobial studies, special attention has been paid to the cytotoxic effects of 25MgHAp stable dispersions and coatings obtained from stable dispersions. Proliferation of human fetal osteoblasts (hFOB 1.19) cells on 25MgHAp suspensions and coatings was determined by MTT assay (Figure 18). The HAp suspension and HAp coatings were used as a reference (Figure 18). An evaluation of hFOB 1.19 cell proliferation was also performed on the glass substrate before coating. Figure 16 shows the viability of hFOB 1.19 cells on substrate, suspensions and coatings. Both the samples in the form of suspensions and those in the form of coatings showed excellent values of viability both at 4 days and at 7 days. As could be seen in the histogram, no major differentiation was observed between the samples in the form of suspension and coatings. Coatings of HAp and 25MgHAp showed a higher growth tendency than the glass substrate before coating. However, in the case of 25MgHAp samples (dispersion or coating) a better cell proliferation compared to the HAp samples (dispersion or coating) was observed. This could be due to the presence of Mg ions in the hydroxyapatite structure.

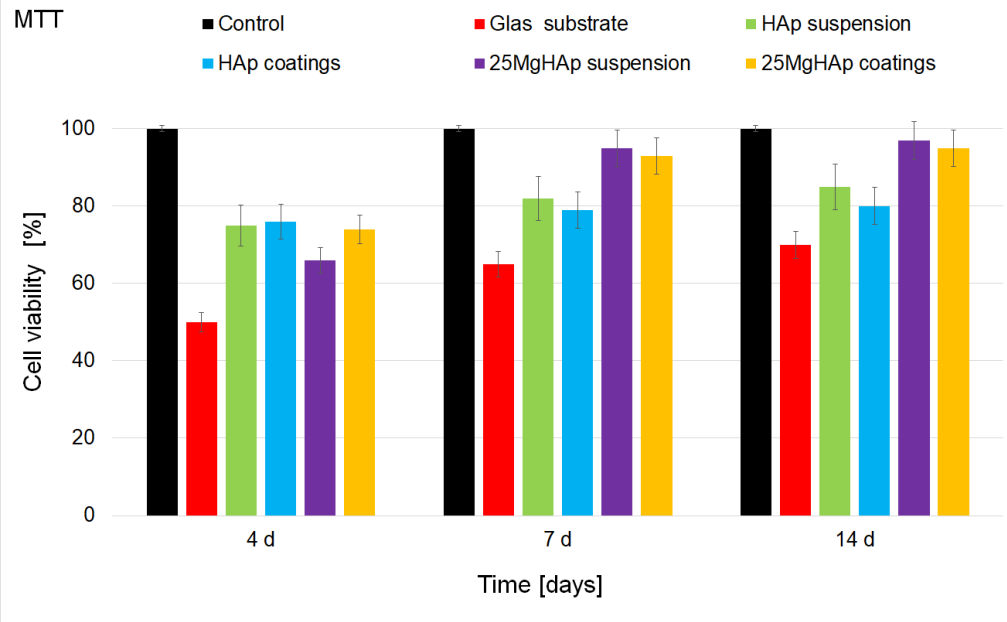

Figure 18. MTT assay for the viability of hOB cells cultured on glass substrate before coating, HA coating, 25MgHAp coating, HAp dispersions, and 25MgHAp dispersions at various incubation periods.

Figure 18 showed that throughout the culture period, the 25MgHAp suspension and coating samples had the highest cell viability values after 4 days, of over 75% ± 10%, while after 14 days, their viability increased to 85% ± 7% compared to the control. The HAp-based samples in the form of suspension and thin layer had a viability of less than 75% ± 10% after 4 days of incubation, reaching about 82% ± 8% after 7 days, while after 14 days, the cell viability was 80% ± 8% for the layers and 85% ± 8% for the sample in the form of suspension. For the uncoated glass substrate, cell viability was 50% ± 5% after 4 days, reaching 65% ± 3% after 7 days and 70% ± 4% after 14 days. After 14 days, the difference between the cell viability of HAp and 25MgHAp samples becomes significantly greater than the cell viability of the uncoated substrate. This behavior shows that both HAp and 25MgHAp samples have very good biocompatible/bioactive properties. The results are in agreement with the studies performed to date, studies showing that hydroxyapatite facilitates the attachment and growth of osteoblastic cells due to its high hydrophilic property [55,56].

The results obtained in our study revealed that the 25MgHAp suspension and 25MgHAp coatings exhibited strong antimicrobial properties by effectively inhibiting the development of *S. aureus* ATCC 25923, *E. coli* ATCC 25922, and *C. albicans* ATCC 9002 CFU microbial strains. The data suggested that the CFU inhibition was pronounced for all tested samples and that was correlated with the incubation time. Nonetheless, the results have emphasized a strong inhibition of CFU/mL of all tested microbial strains from the first 8 h of exposure to both suspensions and coatings. Furthermore, a fungicidal effect as observed in the case of the 25MgHAp suspensions after 48 h of exposure. These findings are in agreement with several other reported data from the literature [24,30,46–48] and demonstrated that, due to their excellent biocompatibility combined with good antimicrobial activity, these compounds could be successfully considered for the development of novel alternative antimicrobial agents for being used in biomedical applications.

On the other hand, an excess of Mg could produce hydroxyl radicals ($^{\bullet}OH$) and superoxide anions (O_2^-), which could cause protein inactivation and even apoptosis [57]. However, taking into account the preferential substitution of Mg in the Ca(II) position in the hydroxyapatite structure [58] the risk of having a larger quantity of magnesium decreases considerably, becoming even non-existent. All coatings manufactured as well as suspension based on HAp and MgHAp provided an excellent environment for proliferation of primary hOB osteoblast cells. In agreement with previous studies [59], the studies using hFOB 1.19 cells revealed that the presence of Mg in HAp structure by preferential

substitution of Mg ions in the Ca^{2+} position, stabilized the cell-material interface by improving attachment and cell growth.

The results obtained in our studies are in agreement with the existing studies regarding magnesium doped hydroxyapatite-based materials [60–63]. The data suggested that the presence of magnesium ions have considerably enhanced the biocompatibility of HAp. Moreover, compared to other ions that were investigated as dopants for hydroxyapatites, magnesium presented HAp with significantly increased biological properties as well as mechanical strength and dissolution rate [60–63]. Furthermore, in their studies on "biomimetic Mg-substituted hydroxyapatite: from synthesis to in vivo behavior" [63], the authors showed that both the biocompatibility and the resorption of Mg-substituted HAp were considerably enhanced compared to stoichiometric HA by conducting in vivo tests on New Zealand White rabbits. Similar results were obtained in the study on "osteoblastic cell response on fluoridated hydroxyapatite coatings: the effect of magnesium incorporation" [64], which reported that HAp and MgHAp coatings effectively enhanced the bioactivity and biocompatibility of a Ti substrate. Furthermore, the authors of the paper "Biomimetic apatite formation on chemically treated titanium" [65] reported in their study that magnesium doped HAp-coated surfaces promoted the in vitro osteogenic differentiation of pre-osteoblasts and improved the implant osseointegration starting with the early stages of bone healing compared with a pure HAp-coated surface. As could be seen, the 25MgHAp suspension showed a much better stability than 10MgHAp suspension. The stability parameter of the 25MgHAp suspensions was $s = 0.019\ s^{-1}$ compared to $0.087\ s^{-1}$ for the 10MgHAp suspensions, while for pure water, the value of s is 0. On the other hand, in our previous studies on MgHAp nanoparticle suspensions in conjunction with a dextran and thyme suspension, the value of the stability parameter was 1.35×10^{-5} (1/s). An increase in the stability of the 25MgHA suspensions can lead to much more stable suspensions in the case of MgHAp nanoparticle suspensions in conjunction with a dextran and thyme suspension, when the 25MgHAp suspensions are conjugated with the different biopolymers and/or essential oils antimicrobial properties. On the other hand, the antimicrobial properties of coatings obtained using 25MgHAp suspensions were much better than in the case of 10MgHAp coatings, referring to the same microbial strains. By increasing the antimicrobial properties and the stability of the suspensions, more effective coatings can be made that will contribute to the prevention of post-surgical infections. It is well-known that coatings with effective antimicrobial action could reduce the risk of postoperative bone infections [66] by preventing the proliferation of bacteria and the development of biofilm.

The 25 MgHAp suspension and coatings were studied to establish the good equilibrium between the antimicrobial properties and cytocompatibility. Moreover, in this study it was shown that the Mg content of the analyzed samples (suspension and coatings) can contribute both to the increase of biocompatibility (it is not-toxic to cells) and to antimicrobial activity.

4. Conclusions

Magnesium doped hydroxyapatite coatings were prepared using a dip coating procedure using 25MgHAp suspensions obtained by an adapted co-precipitation method. The 25MgHAp suspensions were evaluated for their stability using ultrasound measurements, zeta potential (ZP) and dynamic light scattering (DLS) studies. The results obtained in the present study comparative with our previous studies demonstrated that the stability of the samples is strongly influenced by the magnesium concentration. Information regarding the morphology of the samples obtained by SEM and TEM revealed that the 25MgHAp particles in suspension presented spherical structures and nanometric size. On the other hand, the 25MgHAp coatings obtained by dip coating method were investigated by SEM, EDX mapp analysis, and AFM. The results have emphasized that the coatings presented a homogeneous surface and clearly confirmed the presence of Ca, P, Mg, and O elements in the composition of the investigated samples. Moreover, the AFM surface topography of the coatings revealed that the 25MgHAp coatings exhibit the morphology of a uniform deposited layer with no cracks or fissures. Furthermore, the antimicrobial activity of both 25MgHAp suspensions and

coatings were investigated using the reference microbial strain *Staphylococcus aureus* ATCC 25923, *Escherichia coli* ATCC 25922 and *Candida albicans* ATCC 90029 at various time intervals. The results of the antimicrobial assays suggested that all the samples started inhibiting the tested microbial strains development from 8 h of incubation. In addition, it revealed that the 25MgHAp suspensions and 25MgHAp coatings exhibited strong antimicrobial properties by effectively inhibiting the development of *S. aureus* ATCC 25923, *E. coli* ATCC 25922, and *C. albicans* ATCC 9002 CFU microbial strains and that their antimicrobial activity was influenced by the incubation time. This work proved that Mg ions doped in hydroxyapatite nanoparticles none affected hFOB 1.19 cell behavior. Amounts of Mg in the suspension and coating samples revealed a good equilibrium between the antimicrobial properties and cytocompatibility. Moreover, the presence of Mg ions in hydroxyapatite structure contributed to the increase of biocompatibility. The results presented in the present study highlighted that the coatings obtained from 25MgHAp suspensions by dip coating procedure have good antimicrobial properties, which makes them ideal candidates for the development of novel antimicrobial medical devices.

Author Contributions: Conceptualization, D.P. and M.V.P.; Methodology, D.P., M.V.P., and S.L.I.; Software, M.V.P.; Validation, D.P., M.M.-H., and M.V.P.; Formal Analysis, D.P., S.L.I., M.V.P., M.M.-H., C.M., and N.B.; Investigation, M.V.P., S.L.I., D.P., C.M., and N.B.; Resources, D.P., C.M., M.V.P., M.M-H., and N.B.; Data Curation, D.P., S.L.I., and M.V.P.; Writing—Original Draft Preparation, D.P., S.L.I., M.V.P., M.M.-H., and N.B.; Writing—Review & Editing, D.P., S.L.I., and M.V.P.; Visualization, D.P., C.M., S.L.I., M.V.P., M.M.-H., and N.B.; Supervision, D.P., M.V.P., M.M.-H., and N.B.; Project Administration, M.V.P.; Funding Acquisition, D.P. All authors have read and agreed to the published version of the manuscript.

Funding: This research was partially funded by the Romanian Ministry of Research and Innovation through the projects PN-III-P1-1.2-PCCDI-2017-0629/contract No. 43PCCDI/2018, PN-III-P1-1.2-PCCDI-2017-0062/contract No. 58PCCDI/2018/component project No. 2 and Core Program PN19-030101 (contract 21N/2019).

Acknowledgments: We thank C.C. Negrila for his help in XPS data acquisition. This work was supported by the Romanian Ministry of Research and Innovation through the projects PN-III-P1-1.2-PCCDI-2017-0629/contract No. 43PCCDI/2018, PN-III-P1-1.2-PCCDI-2017-0062/contract No. 58PCCDI/2018/component project No. 2 and Core Program PN19-030101 (contract 21N/2019).

Conflicts of Interest: The authors declare no conflict of interest.

References

1. Dasgupta, S.; Bandyopadhyay, A.; Bose, S. Zn and Mg Doped Hydroxyapatite Nanoparticles for Controlled Release of Protein. *Langmuir* **2010**, *26*, 4958–4964. [CrossRef] [PubMed]
2. Aina, V.; Lusvardi, G.; Annaz, B.; Gibson, I.R.; Imrie, F.E.; Malavasi, G.; Menabue, L.; Cerrato, G.; Martra, G. Magnesium-and strontium-co-substituted hydroxyapatite: The effects of doped-ions on the structure and chemico-physical properties. *J. Mater. Sci. Mater. Med.* **2012**, *23*, 2867–2879. [CrossRef] [PubMed]
3. Mróz, W.; Bombalska, A.; Burdynska, S.; Jedynski, M.; Prokopiuk, A.; Budner, B.; S'lósarczyk, A.; Zima, A.; Menaszek, E.; S'cisłowska-Czarnecka, A.; et al. Structural studies of magnesium doped hydroxyapatite coatings after osteoblast culture. *J. Mol. Struct.* **2010**, *977*, 145–152. [CrossRef]
4. Mroz, W.; Budner, B.; Syroka, R.; Niedzielski, K.; Golanski, G.; Slosarczyk, A.; Schwarze, D.; Douglas, T.E.L. In vivo implantation of porous titanium alloy implants coated with magnesium-doped octacalcium phosphate and hydroxyapatite thin films using pulsed laser deposition. *J. Biomed. Mater. Res. B* **2014**, *103*, 151–158. [CrossRef]
5. Iconaru, S.L.; Prodan, A.M.; Turculet, C.S.; Beuran, M.; Ghita, R.V.; Costescu, A.; Groza, A.; Chifiriuc, M.C.; Chapon, P.; Gaiaschi, S.; et al. Enamel Based Composite Layers Deposited on Titanium Substrate with Antifungal Activity. *J. Spectrosc.* **2016**, *2016*, 4361051. [CrossRef]
6. Sartori, M.; Giavaresi, G.; Tschon, M.; Martini, L.; Dolcini, L.; Fiorini, M.; Pressato, D.; Fini, M. Long-term in vivo experimental investigations on magnesium doped hydroxyapatite bone substitutes. *J. Mater. Sci. Mater. Med.* **2014**, *25*, 1495–1504. [CrossRef]
7. Greenwald, A.S.; Boden, S.; Goldberg, V.M.; Khan, Y.; Laurencin, C.T.; Rosier, R.N. Bone-graft substitutes: Facts, fictions, and applications. *J. Bone Jt. Surg. Am.* **2001**, *83*, 98–103. [CrossRef]
8. US Bone Grafts Industry. Global Industry Analysts Inc. 2011. Available online: http://www.reportlinker.com/p0119465-summary/World-Bone-Grafts-Market.html (accessed on 21 January 2020).

9. Zimmermann, G.; Moghaddam, A. Allograft bone matrix versus synthetic bone graft substitutes. *Injury* **2011**, *42*, S16–S21. [CrossRef]
10. Giannoudis, P.V.; Dinopoulos, H.; Tsiridis, E. Bone substitutes: An update. *Injury* **2005**, *36*, S20–S27. [CrossRef]
11. Oliveira, A.L.; Mano, J.F.; Reis, R.L. Nature-inspired calcium phosphate coatings: Present status and novel advances in the science of mimicry. *Curr. Opin. Solid State Mater. Sci.* **2003**, *7*, 309–318. [CrossRef]
12. Predoi, D.; Iconaru, S.L.; Buton, N.; Badea, M.L.; Marutescu, L. Antimicrobial Activity of New Materials Based on Lavender and Basil Essential Oils and Hydroxyapatite. *Nanomaterials* **2018**, *8*, 291. [CrossRef] [PubMed]
13. Albee, F.H.; Morrison, H.F. Studies in bone growth triple calcium phosphate as a stimulus to osteogenesis. *Ann. Surg.* **1920**, *71*, 32–39. [PubMed]
14. Nery, E.B.; Lynch, K.L.; Hirthe, W.M.; Mueller, K.H. Bioceramic Implants in Surgically Produced Infrabony Defects. *J. Periodontol.* **1975**, *46*, 328–347. [CrossRef] [PubMed]
15. Zhou, H.; Lee, J. Nanoscale hydroxyapatite particles for bone tissue engineering. *Acta Biomater.* **2011**, *7*, 2769–2781. [CrossRef] [PubMed]
16. Yana, Y.; Dinga, Q.; Huanga, Y.; Hana, S.; Panga, X. Magnesium substituted hydroxyapatite coating on titanium with nanotublar TiO_2 intermediate layer via electrochemical deposition. *Appl. Surf. Sci.* **2014**, *305*, 77–85.
17. Shepherd, J.H.; Shepherd, D.V.; Best, S.M. Substituted hydroxyapatites for bonerepair. *J. Mater. Sci. Mater. Med.* **2012**, *23*, 2335–2347. [CrossRef]
18. Iconaru, S.L.; Prodan, A.M.; Buton, N.; Predoi, D. Structural Characterization and Antifungal Studies of Zinc-Doped Hydroxyapatite Coatings. *Molecules* **2017**, *22*, 604. [CrossRef]
19. Ciobanu, C.S.; Iconaru, S.L.; Popa, C.L.; Motelica-Heino, M.; Predoi, D. Evaluation of samarium doped hydroxyapatite, ceramics for medical application: Antimicrobial activity. *J. Nanomater.* **2015**, *2015*, 849216. [CrossRef]
20. Predoi, D.; Iconaru, S.L.; Predoi, M.V. Bioceramic layers with antifungal properties. *Coatings* **2018**, *8*, 276. [CrossRef]
21. Nagyné-Kovács, T.; Studnicka, L.; Kincses, A.; Spengler, G.; Molnár, M.; Tolner, M.; Lukács, I.E.; Szilágyi, I.M.; Pokol, G. Synthesis and characterization of Sr and Mg-doped hydroxyapatite by a simple precipitation method. *Ceram. Int.* **2018**, *44*, 22976–22982. [CrossRef]
22. Predoi, D.; Iconaru, S.L.; Deniaud, A.; Chevallet, M.; Michaud-Soret, I.; Buton, N.; Prodan, A.M. Textural, Structural and Biological Evaluation of Hydroxyapatite Doped with Zinc at Low Concentrations. *Materials* **2017**, *10*, 229. [CrossRef] [PubMed]
23. Turculet, C.S.; Prodan, A.M.; Negoi, I.; Teleanu, G.; Popa, M.; Andronescu, E.; Beuran, M.; Stanciu, G.A.; Hristu, R.; Badea, M.L.; et al. Preliminary Evaluation Of The Antifungal Activity Of Samarium Doped Hydroxyapatite Thin Films. *Rom. Biotechnol. Lett.* **2018**, *23*, 13928–13932. [CrossRef]
24. Predoi, D.; Iconaru, S.L.; Predoi, M.V.; Stan, G.E.; Buton, N. Synthesis, Characterization, and Antimicrobial Activity of Magnesium-Doped Hydroxyapatite Suspensions. *Nanomaterials* **2019**, *9*, 1295. [CrossRef] [PubMed]
25. Cacciotti, I.; Bianco, A.; Lombardi, M.; Montanaro, L. Mg-substituted hydroxyapatite nanopowders: Synthesis, thermal stability and sintering behavior. *J. Eur. Ceram. Soc.* **2009**, *29*, 969–2978. [CrossRef]
26. Adzila, S.; Murad, M.C.; Sopyan, I. Doping metal into calcium phosphate phase for better performance of bone implant materials. *Rec. Pat. Mater. Sci.* **2012**, *5*, 18–47. [CrossRef]
27. Serre, C.M.; Papillard, M.; Chavassieux, P.; Voegel, J.C. Influence of magnesium substitution on a collagen-appatite biomaterial on the production of calcifying matrix by human osteoblasts. *J. Biomed. Mater. Res.* **1998**, *42*, 626–633. [CrossRef]
28. Dhert, W.J.A.; Klein, C.P.; Jansen, J.A. A histological and histomorphometrical investigation of fluorapatite magnesiumwhitlockite, and hydroxylapatite plasma-sprayed coatings in goats. *J. Biomed. Mater. Res.* **1993**, *27*, 127–138. [CrossRef]
29. Webster, T.J.; Ergun, C.; Doremus, R.H.; Bizios, R. Hydroxylapatie with substituted magnesium, zinc, cadmium and yttrium. II. Mechanisms of osteoblast adhesion. *J. Biomed. Mater. Res.* **2002**, *59*, 312–317. [CrossRef]

30. Iconaru, S.L.; Predoi, M.V.; Motelica-Heino, M.; Predoi, D.; Buton, N.; Megier, C.; Stan, G.E. Dextran-Thyme Magnesium-Doped Hydroxyapatite Composite Antimicrobial Coatings. *Coatings* **2020**, *10*, 57. [CrossRef]
31. Mishra, U. Development of Cobalt-Magnesium Doped Hydroxyapatite for Bone Tissue Engineering Application. Bachelor's Thesis, Department of Biotechnology and Medical EngineeringNational Institute of Technology, Rourkela, India, 2013.
32. Kulanthaivel, S.; Mishraa, U.; Agarwala, T.; Girib, S.; Pala, K.; Pramanika, K.; Banerjeea, I. Improving the osteogenic and angiogenic properties of synthetic hydroxyapatite by dual doping of bivalent cobalt and magnesium ion. *Ceram. Int.* **2015**, *41*, 11323–11333. [CrossRef]
33. Kalita, S.J.; Bhatt, H.A. Nanocrystalline hydroxyapatite doped with magnesium and zinc: Synthesis and characterization. *Mater. Sci. Eng. C* **2007**, *27*, 837–848. [CrossRef]
34. Boanini, E.; Torricelli, P.; Fini, M.; Sima, F.; Serban, N.; Mihailescu, I.N.; Bigi, A. Magnesium and strontium doped octacalcium phosphate thin films by matrix assisted pulsed laser evaporation. *J. Inorg. Biochem.* **2012**, *107*, 65–72. [CrossRef] [PubMed]
35. Ciobanu, C.S.; Iconaru, S.L.; Massuyeau, F.; Constantin, L.V.; Costescu, A.; Predoi, D. Synthesis, structure, and luminescent properties of europium-doped hydroxyapatite nanocrystalline powders. *J. Nanomater.* **2012**, *2012*, 942801. [CrossRef]
36. Predoi, D.; Iconaru, S.L.; Predoi, M.V.; Motelica-Heino, M.; Guegan, R.; Buton, N. Evaluation of Antibacterial Activity of Zinc-Doped Hydroxyapatite Colloids and Dispersion Stability Using Ultrasounds. *Nanomaterials* **2019**, *9*, 515. [CrossRef]
37. Rodriguez, L.; Matoušek, J. Preparation of TiO_2 sol-gel layers on glass. *Ceram. Silik.* **2003**, *47*, 28–31.
38. Prodan, A.M.; Iconaru, S.L.; Predoi, M.V.; Predoi, D.; Motelica-Heino, M.; Turculet, C.S.; Beuran, M. Silver-Doped Hydroxyapatite Thin Layers Obtained by Sol-Gel Spin Coating Procedure. *Coatings* **2020**, *10*, 14. [CrossRef]
39. Yamaguchi, M. Role of zinc in bone formation and bone resorption. *J. Trace Elem. Exp. Med.* **1998**, *11*, 119–135. [CrossRef]
40. ImageJ Website. Available online: http://imagej.nih.gov/ij (accessed on 10 January 2018).
41. Predoi, D.; Vatasescu-Balcan, R.A. Osteoblast interaction with iron oxide nanoparticles coated with dextrin in cell culture. *J. Optoelectron. Adv. Mat.* **2008**, *10*, 152–157.
42. Kadu, P.J.; Kushare, S.S.; Thacker, D.D.; Gattani, S.G. Enhancement of oral bioavailability of atorvastatin calcium by self-emulsifying drug delivery systems (SEDDS). *Pharm. Dev. Technol.* **2011**, *16*, 65–74. [CrossRef]
43. Mohapatra, S.S.; Ranjan, S.; Thomas, S. *Characterization and Biology of Nanomaterials for Drug Delivery Nanoscience and Nanotechnology in Drug Delivery A volume in Micro and Nano Technologies*; Elsevier: Amsterdam, The Netherlands, 2019; ISBN 978-0-12-814031-4. [CrossRef]
44. Joseph, E.; Singhvi, G. Chapter 4—Multifunctional nanocrystals for cancer therapy: A potential nanocarrier. In *Nanomaterials for Drug Delivery and Therapy*; Elsevier: Amsterdam, The Netherlands, 2019; pp. 91–116. [CrossRef]
45. Ley, L.; McFeely, F.R.; Kowalczyk, S.P.; Jenkin, J.G.; Shirley, D.A. Many-body effects in x-ray photoemission from magnesium. *Phys. Rev. B* **1975**, *11*, 600e12. [CrossRef]
46. Ardizzone, S.; Bianchi, L.; Fadoni, M.; Vercelli, B. Magnesium salts and oxide: An XPS overview. *Appl. Surf. Sci.* **1997**, *119*, 253–259. [CrossRef]
47. Friedrichs, O.; Sánchez-López, J.C.; López-Cartes, C.; Dornheim, M.; Klassen, T.; Fernandez, A. Chemical and microstructural study of the oxygen passivation behaviour of nanocrystalline Mg and MgH2. *Appl. Surf. Sci.* **2006**, *252*, 2334e45. [CrossRef]
48. Zhang, D.; Lepparanta, O.; Munukka, E.; Ylanen, H.; Viljanen, M.K.; Eerola, E.; Hupa, M.; Hupa, L. Antibacterial effects and dissolution behavior of six bioactive glasses. *J. Biomed. Mater. Res. A* **2010**, *93*, 475–483. [CrossRef]
49. Mortazavi, V.; Nahrkhalaji, M.M.; Fathi, M.H.; Mousavi, S.B.; Esfahani, B.N. Antibacterial effects of sol-gel-derived bioactive glass nanoparticle on aerobic bacteria. *J. Biomed. Mater. Res. A* **2010**, *94*, 160–168. [CrossRef] [PubMed]
50. Zhu, L.; Wana, P.; Duanb, J.; Tana, L.; Yanga, K. An alternative magnesium based root canal disinfectant: Preliminary study of its efficacy against *Enterococcus faecalis* and *Candida albicans* in vitro. *Prog. Nat. Sci. Mater. Int.* **2014**, *24*, 441–445. [CrossRef]

51. Leung, Y.H.; Ng, A.M.; Xu, X.; Shen, Z.; Gethings, L.A.; Wong, M.T.; Chan, C.M.; Guo, M.Y.; Ng, Y.H.; Djurišić, A.B.; et al. Mechanisms of antibacterial activity of MgO: Non-ROS mediated toxicity of MgO nanoparticles towards *Escherichia coli*. *Small* **2013**, *10*, 1171–1183. [CrossRef] [PubMed]
52. Manke, A.; Wang, L.; Rojanasakul, Y. Mechanisms of nano-particle-induced oxidative stress and toxicity. *BioMed Res. Int.* **2013**, *2013*, 942916. [CrossRef]
53. Sabella, S.; Carney, R.P.; Brunetti, V.; Malvindi, A.M.; Al-Juffali, N.; Vecchio, G.; Janes, S.M.; Bakr, O.M.; Cingolani, R.; Stellacci, F.; et al. A general mechanism for in-tracellular toxicity of metal-containing nanoparticles. *Nanoscale* **2014**, *6*, 7052–7061. [CrossRef]
54. Ghobadian, M.; Nabiuni, M.; Parivar, K.; Fathi, M.; Pazooki, J. Toxic effects of magnesium oxide nanoparticles on early developmental and larval stages of zebrafish (Danio rerio). *Ecotoxicol. Environ. Saf.* **2015**, *122*, 260–267. [CrossRef]
55. Thian, E.S.; Ahmad, Z.; Huang, J.; Edirisinghe, M.J.; Jayasinghe, S.N.; Ireland, D.C.; Brooks, R.A.; Rushton, N.; Bonfield, W.; Best, S.M. The role of surface wettability and surface charge of electrosprayed nanoapatites on the behaviour of osteoblasts. *Acta Biomater.* **2010**, *6*, 750–755. [CrossRef]
56. Kilpadi, K.L.; Chang, P.-L.; Bellis, S.L. Hydroxylapatite binds more serum proteins, purified integrins, and osteoblast precursor cells than titanium or steel. *J. Biomed. Mater. Res.* **2001**, *57*, 258–267. [CrossRef]
57. Hayyan, M.; Hashim, M.A.; AlNashef, I.M. Superoxide Ion: Generation and Chemical Implications. *Chem. Rev.* **2016**, *116*, 3029–3085. [CrossRef] [PubMed]
58. Acton General, Q.A. (Ed.) *Magnesium Compounds—Advances in Research and Application*, 2013 ed.; Scholarly Editions: Atlanta, GA, USA, 2013; p. 333.
59. Xue, W.; Dahlquist, K.; Banerjee, A.; Bandyopadhyay, A.; Bose, S. Synthesis and characterization of tricalcium phosphate with Zn and Mg based dopants. *J. Mater. Sci. Mater. Med.* **2008**, *19*, 2669–2677. [CrossRef] [PubMed]
60. Yamasaki, Y.; Yoshida, Y.; Okazaki, M.; Shimazu, A.; Kubo, T.; Akagawa, Y.; Uchida, T. Action of FGMgCO3Ap–collagen composite in promoting bone formation. *Biomaterials* **2003**, *24*, 4913–4920. [CrossRef]
61. Zhao, S.F.; Jiang, Q.H.; Peel, S.; Wang, X.X.; He, F.M. Effects of magnesium-substituted nanohydroxyapatite coating on implant osseointegration. *Clin. Oral Implant. Res.* **2013**, *24*, 34–41. [CrossRef] [PubMed]
62. Yamasaki, Y.; Yoshida, Y.; Okazaki, M.; Shimazu, A.; Uchida, T.; Kubo, T.; Akagawa, Y.; Hamada, Y.; Takahashi, J.; Matsuura, N. Synthesis of functionally graded $MgCO_3$ apatite accelerating osteoblast adhesion. *J. Biomed. Mater. Res.* **2002**, *62*, 99–105. [CrossRef] [PubMed]
63. Landi, E.; Logroscino, G.; Proietti, L.; Tampieri, A.; Sandri, M.; Sprio, S. Biomimetic Mg-substituted hydroxyapatite: From synthesis to in vivo behaviour. *J. Mater. Sci. Mater. Med.* **2008**, *19*, 239–247. [CrossRef]
64. Cai, Y.L.; Zhang, J.J.; Zhang, S.; Venkatraman, S.S.; Zeng, X.T.; Du, H.J.; Mondal, D. Osteoblastic cell response on fluoridated hydroxyapatite coatings: The effect of magnesium incorporation. *Biomed. Mater.* **2010**, *5*, 054114. [CrossRef]
65. Jonasova, L.; Muller, F.A.; Helebrant, A.; Strnad, J.; Greil, P. Biomimetic apatite formation on chemically treated titanium. *Biomaterials* **2004**, *25*, 1187–1194. [CrossRef]
66. Monzavi, A.; Eshraghi, S.; Hashemian, R.; Momen-Heravi, F. In vitro and ex vivo antimicrobial efficacy of nano-MgO in the elimination of endodontic pathogens. *Clin. Oral Investig.* **2015**, *19*, 349–356. [CrossRef]